Journal of the Serbian Chemical Society
JSCS-info@shd.org.rs • www.shd.org.rs/JSCS
J. Serb. Chem. Soc. 84 (8) 915–923 (2019)
JSCS–5234
UDC 546.62'47'28+543.42:66.087.3:533.9+544.032.4
Original scientific paper

Spectroscopic study of micro-discharges during plasma electrolytic oxidation of Al–Zn–Si alloy

STEVAN STOJADINOVIĆ* and RASTKO VASILIĆ

University of Belgrade, Faculty of Physics, Studentski trg 12–16, 11000 Belgrade, Serbia

(Received 18 April, accepted 9 May 2019)

Abstract: Plasma electrolytic oxidation (PEO) process of Al–Zn–Si alloy in water solution containing 4 g L^{-1} sodium metasilicate at constant current density of 400 mA cm^{-2} was investigated. The species present in PEO micro--discharges and their ionization stages were identified using optical emission spectroscopy technique. The obtained PEO spectrum consists of atomic/ionic lines originating from the elements present both in the substrate (Al, Zn) and the electrolyte (Na, O, H). Apart from atomic and ionic lines, AlO band at 484.2 nm was also detected. Plasma electron number density diagnostics was performed from the H_β line shape. The electron temperature of 4000±400 K was estimated by measuring the relative line intensities of zinc atomic lines at 481.05 and 636.23 nm. In addition, surface morphology, chemical and phase composition of oxide coatings were investigated by SEM-EDS and XRD. Oxide coating morphology is strongly dependent of PEO time. The elemental components of PEO coatings are Al, Zn, O and Si. The oxide coatings are partly crystallized and mainly composed of gamma phase of Al_2O_3.

Keywords: micro-arc oxidation; anodization; optical emission spectroscopy; plasma temperature; gamma Al_2O_3.

INTRODUCTION

Plasma electrolytic oxidation (PEO), also known as micro-arc oxidation (MAO) or anodic spark deposition (ASD), is a high-voltage anodizing process in which the surface of some metals such as aluminium[1], magnesium[2], titanium[3], tantalum[4], niobium[5], hafnium[6], zinc[7] or their alloys are converted into oxide coatings. PEO process is based on the anodization of metals above the dielectric breakdown voltage of original oxide film (typically from 350 to 600 V). The appearance of plasma is registered in the form of numerous transient short-living micro-discharges generated continuously over the coating surface and accompanied by gas evolution.[8] Micro-discharging happens as a consequence of loss in oxide film's dielectric stability in the region of low conductivity and results in

* Corresponding author. E-mail: sstevan@ff.bg.ac.rs
https://doi.org/10.2298/JSC190418040S

localized high temperature (10^3 to 10^4 K) and high pressure (~10^2 Pa). Various processes including electrochemical, chemical, thermodynamical and plasma-chemical occur at the micro-discharge sites and play an important role in the phase formation, composition and morphology of formed oxide coating. The PEO coatings usually contain crystalline and amorphous phases with constituent species originating both from metal and electrolyte.

The distribution and types of micro-discharges have important effects on the formation mechanism of the resultant oxide coatings. Optical emission spectroscopy (OES) is the most convenient technique for characterization of micro-discharges appearing during the PEO. In general, it has been found that micro-discharge optical emission spectra originate from both the species present in substrate and in electrolyte.[9–28] The most popular application of OES for PEO diagnostics is spectra characterization and observation of temporal evolution of spectral lines in the visible and near UV spectral region. The main obstacle in OES application for PEO characterization comes from space and time inhomogeneity of micro-discharges appearing randomly across the anode surface. The results of relative line intensity measurements of species originating either from the substrate or from the electrolyte have been employed to determine the electron temperature.[3,11,15,19] The spectral line shape analyses of hydrogen Balmer lines or ion lines from the substrate have often been used to estimate the electron number density.[3,6,7,11,12,33] The molecular vibrational temperature was determined from the $B^2\Sigma^+ \rightarrow X^2\Sigma^+$ emission transition of AlO,[13,20] and the $B^1\Sigma^+ \rightarrow X^1\Sigma^+$ emission transition of MgO.[14,20,29]

The present paper describes PEO process of Al–Zn–Si alloy (a nominal composition of 55 % aluminum, 43.5 % zinc and 1.5 % silicon) in sodium metasilicate. Al–Zn–Si alloy has good oxidation resistance, excellent electrochemical protection, good resistance to wet corrosion, and high energy efficiency with superior heat reflection and low heat consumption.[30] Micro-discharge characteristics during PEO process of Al–Zn–Si alloy were investigated by optical emission spectroscopy. Scanning electron microscopy (SEM-EDS) and x-ray diffraction (XRD) served as tools for examining surface morphology, chemical and phase composition of obtained oxide coatings.

EXPERIMENTAL

Rectangular samples of dimensions 25 mm×5 mm of Al–Zn–Si alloy (55 % Al, 43.5 % Zn, 1.5 % Si) were used as working electrodes, while two platinum wires (5 cm long and 1 mm in diameter) were used as cathodes in experiments. The working electrodes were sealed with insulation resin leaving only an active surface area of 15×5 mm exposed to the electrolyte. The PEO process took place in an electrolytic cell with flat quartz glass windows.[31] PEO was performed under constant current density of 400 mA cm^{-2}, while duration of PEO process was varied up to 15 min. A water solution of 4 g L^{-1} $Na_2SiO_3 \cdot 5H_2O$ was used as the electrolyte. During the PEO, the electrolyte circulated through chamber–reservoir system and the temperature of the electrolyte was maintained at 20±1 °C.

Spectral measurements during PEO were taken on a spectrometer system based on the intensified charge coupled device (ICCD). Optical detection system consisted of a large-aperture achromatic lens, a 0.3 m Hilger spectrometer (diffraction grating 1200 grooves/mm and inverse linear dispersion of 2.7 nm mm^{-1}), and a very sensitive PI–MAX ICCD thermoelectrically cooled camera (–40 °C) with high quantum efficiency manufactured by Princeton Instruments. The CCD chip consisted of 430×256 active pixels, each approximately 26 μm ×26 μm. The system was used with several grating positions with overlapping wavelength range of 5 nm. Spectra were recorded in segments of 43 nm and the whole spectral range was obtained by adding one spectra interval to the previous one.

The surface morphology of obtained coatings was observed by a scanning electron microscope (SEM, JEOL 840A). The surface chemical composition of coatings was examined by an energy dispersive spectrometer (EDS, Oxford) attached to the SEM. Crystal phase identification was performed via X-ray diffraction (XRD) by using a Rigaku Ultima IV diffractometer with Ni-filtered CuKα radiation (λ = 1.54178 Å) source. The XRD data in the 2θ range from 25 to 75° were collected in a scanning mode with a step size of 0.02° and a scanning rate of 2° min^{-1}.

RESULTS AND DISCUSSION

Spectroscopy characterization of PEO process

Voltage of anodization *versus* time and luminescence intensity at 500 nm *versus* time characteristics during anodization of Al–Zn–Si alloy in water solution containing 4 g L^{-1} $Na_2SiO_3{\cdot}5H_2O$ at current density of 400 mA cm^{-2} are shown in Fig. 1. During the first 50 s (stage I), the process is similar to conventional anodizing and in this period relatively compact barrier oxide film is formed. Uniform film thickening is terminated by the dielectric breakdown, coupled with visible micro-discharges evenly distributed over the surface (stage II). First small micro-discharges are visible at 450 V (beginning of PEO process) and after this the luminescence intensity starts to increase.

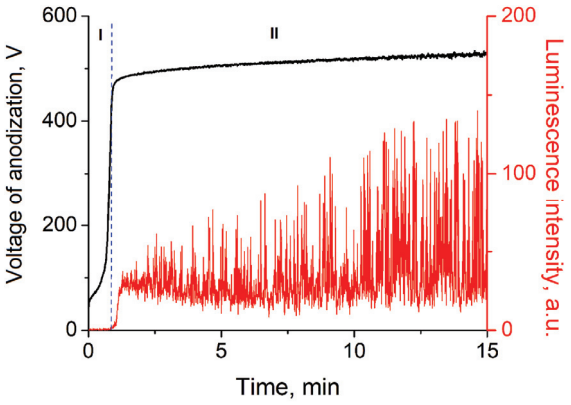

Fig.1. Time variation of voltage of anodization and luminescence intensity at 500 nm during the anodization of Al–Zn–Si alloy in sodium metasilicate.

Typical optical emission spectrum of PEO micro-discharges in the spectral range from 375 to 850 nm is shown in Fig. 2a. Atomic and ionic lines were iden-

tified using the NIST online spectral database.[32] The strongest observed lines originate from the electrolyte and belong to Na I at 588.99 and 589.59 nm and H I at 656.28 nm (Balmer line H_α). We have also detected the following relatively strong lines: Balmer line H_β (486.13 nm), O I at 715.67 nm, three lines of O I at 794.75, 795.08 and 795.22 nm, three lines of O I at 844.62, 844.64 and 844.68 nm from the electrolyte, two lines of Al I at 394.40 and 396.15 nm, and four lines of Zn I at 468.01, 472.21, 480.01 and 636.23 from the substrate. In afore mentioned results notation I and II refers to neutral atoms and single ionized atoms, respectively. The continuum emission between 375 and 850 nm results from collision–radiative recombination of electrons and bremsstrahlung radiation.[28] Detailed optical emission spectra in the spectral range from 400 to 500 nm (Fig. 2b) and from 600 to 840 nm (Fig. 2c) shows many O I, Na I, O II, Zn II and Al II lines. Apart from atomic and ionic lines, AlO band at 484.2 nm was also detected.

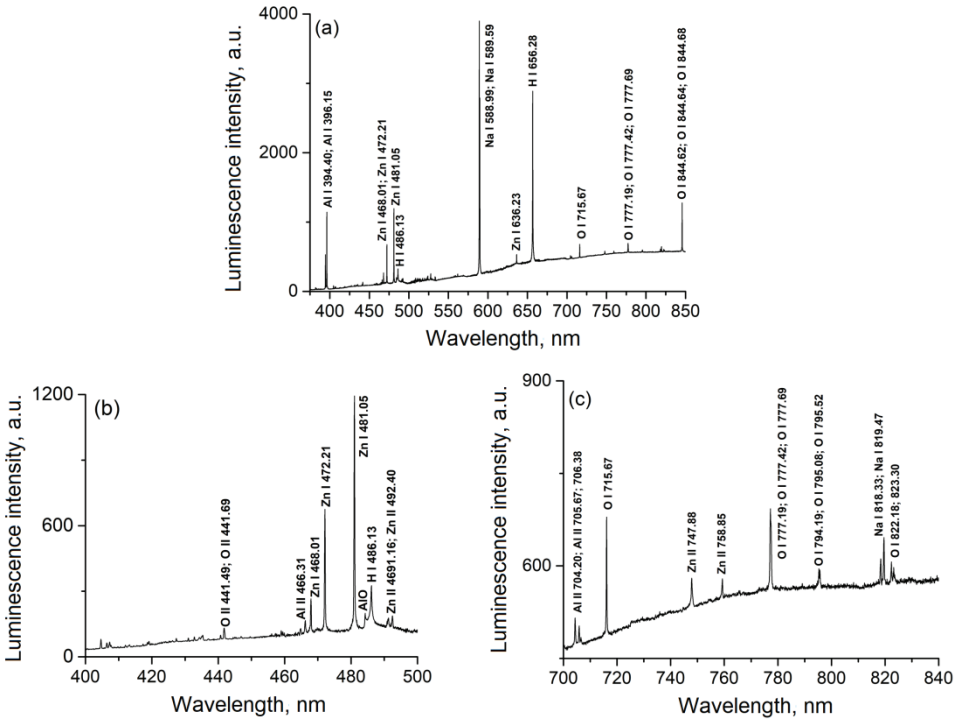

Fig. 2. Optical emission spectra obtained during the PEO in the range of: a) 375–850 nm; b) 400–500 nm; c) 700–840 nm.

For electron number density measurements broadened profile of Balmer H_β line was used. Balmer line H_α is very intensive in PEO process and therefore strongly self-absorbed. For this reason H_α is not suitable for the spectral line shape analysis.[10,11] Analysis of the Balmer H_β line profile during PEO of different

metals showed that H_β line shape can be properly fitted only if two Lorentzian profiles are used.[3,6,7,11,12,33] These Lorentzian profiles correspond to electron number densities of about 1.0×10^{15} and 2.2×10^{16} cm^{-3}. In our case, the lower part of the H_β line is distorted by AlO band (Fig. 2b). In spite of interference with AlO molecular band, the full width at half maximum (FWHM) for the upper part of the profile, after correction by subtracting the instrumental FWHM from the observed, was estimated at about 0.5 nm, corresponding to electron number density of about 3.6×10^{15} cm^{-3}.

For electron temperature (T_e) measurements relative line intensities were used. This temperature is assumed to be equal to electron excitation temperature, measured from relative line intensities. For the application of this assumption one must be sure that energy levels used for T_e measurement are populated in accordance with Boltzmann equilibrium distribution, *i.e.*, that the upper energy level of the spectral line used is above the lowest level determined by partial local thermal equilibrium (PLTE) condition, which is generally the case for plasma electrolytic oxidation.[11]

The relative line intensities of the same atomic species can be used to calculate T_e using the equation:[7]

$$T_e = \frac{E_{m(2)} - E_{m(1)}}{k(\ln I_1 A_{mn(2)} g_{m(2)} \lambda_{o(1)} / I_2 A_{mn(1)} g_{m(1)} \lambda_{o(2)})} \quad (1)$$

where k is the Boltzmann constant, I_1 and I_2 are relative line intensities of the same species, $A_{mn(i)}$ are the transition probabilities, m is the upper and n is the lower level of the respective lines, $g_{m(i)}$ are the statistical weights of the upper level, $E_{m(i)}$ are energies of the upper levels of the lines and $\lambda_{o(i)}$ are the wavelengths of the line centers in vacuum. For T_e measurement we have used Zn I lines (Table I) at 481.05 and 636.23 nm.

TABLE I. The list of Zn I lines used for the calculation of T_e: λ-wavelength, g_m-statistical weight of upper energy level, A_{mn}-transition probability

Line	λ_o / nm	Transition	g_m	Energy, eV	A_{mn} / 10^7 s^{-1}
Zr I	481.05	$4s5s\,^3S_1 \rightarrow 4s4p\,^3P_2$	3	6.654	7.00
Zr I	636.23	$4s5d\,^1D_2 \rightarrow 4s4p\,^1P_1$	5	7.774	4.65

The Balmer lines were ruled out for T_e measurement because H_α is self-absorbed while H_β interferes with AlO band. The Al I lines are also not convenient. Two strong resonance lines Al I 396.1 and 394.4 nm belong to the same multiplet and energy spread of upper energy levels is small, thus introducing a large error in T_e measurement. The O I lines are also excluded for T_e measurement on the basis of similar arguments used for aluminum lines.

Difficulty in estimation of T_e using Eq. (1) is related to the question whether T_e in PEO is measured from the same plasma region and in the same time of micro-discharge evolution. Since it is not possible to perform space and time resolved micro-discharge PEO diagnostics with presently available plasma diagnostic techniques, T_e is measured in a standard way from time integrated relative line intensities. We have performed a series of measurements with different integration times and obtained T_e in the range 4000±400 K.

Morphology, chemical, and phase composition of PEO coatings

Fig. 3 shows the surface morphology evolution of the coatings formed by PEO of Al–Zn–Si alloy.

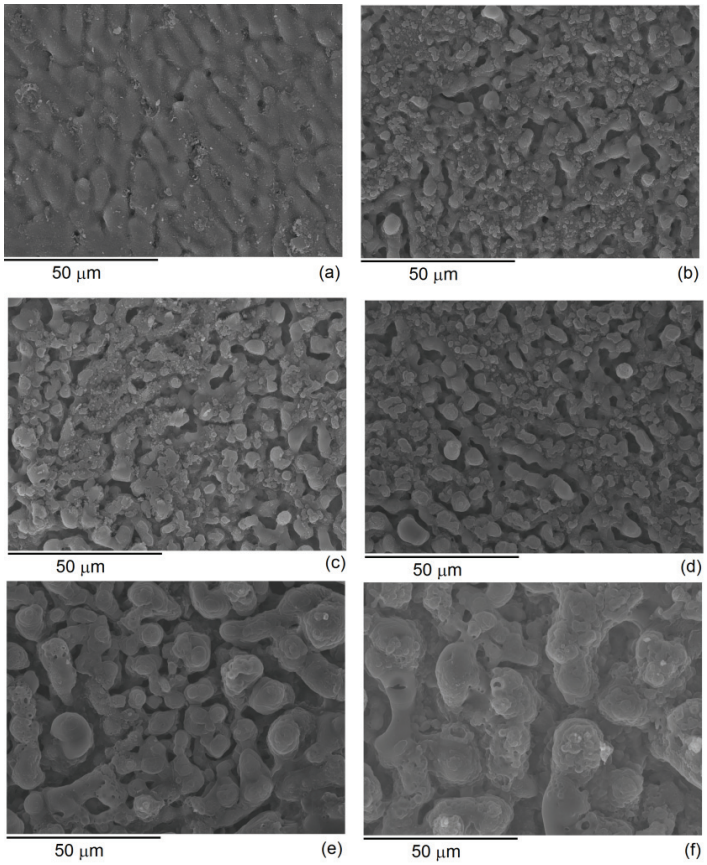

Fig. 3. SEM micrographs of oxide coatings formed at various stages of PEO process: a) 1, b) 2, c) 3, d) 5, e) 10 and f) 15 min.

The coatings show a typical structure formed by PEO, with a number of pores with different diameters and shapes as well as regions resulting from the

rapid cooling of molten material. During the PEO, melted components from substrate enter the micro-discharge channels and react with electrolyte components. Reaction products are ejected from active micro-discharge channels onto the coating surface where they rapidly solidify in contact with the low temperature electrolyte and in that way increase the coating thickness around the channels. At last, micro-discharge channels get cooled and the reaction products are deposited onto its walls.

Results of the EDS analyses of surface coatings in Fig. 3 and the XRD patterns of oxide coatings obtained after various PEO times are shown are Fig. 4. The main elements of the coatings are Al, Zn, Si and O. The oxide coatings are partly crystallized and mainly composed of gamma phase of Al_2O_3.

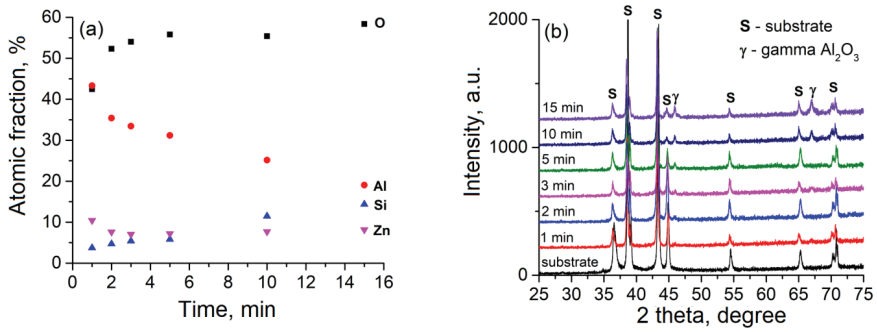

Fig 4. a) EDS analysis of surface coatings in Fig. 3; b) XRD patterns of oxide coatings formed at various stages of PEO process.

CONCLUSIONS

We have studied plasma electrolytic oxidation (PEO) process of Al–Zn–Si alloy in sodium metasilicate. The following conclusions were drawn:

– The species that were identified in optical emission spectrum of micro-discharges originate either from Al–Zn–Si alloy electrode or from the electrolyte. The optical emission spectroscopy measurements based on spectral line shape and line intensity analysis were applied to determine electron number density and electron temperature of plasma micro-discharges. The analysis of hydrogen Balmer line H_β shows that the electron number density of plasma micro-discharges is about 3.6×10^{15} cm^{-3}. The electron temperature of plasma micro-discharges is estimated at about 4000±400 K from the line intensity of zinc atomic lines at 481.05 and 636.23 nm.

– The surface morphology is dependent on PEO time. The main elemental components of PEO coatings are Al, Zn, Si and O. The oxide coatings are partly crystallized and mainly composed of gamma phase of Al_2O_3.

Acknowledgements. This work is supported by the Ministry of Education, Science and Technological Development of the Republic of Serbia under project No. 171035 and by the

European Union Horizon 2020 research and innovation program under the Marie Sklodowska-Curie grant agreement No. 823942.

ИЗВОД

СПЕКТРОСКОПСКА СТУДИЈА МИКРО-ПРАЖЊЕЊА У ТОКУ ПЛАЗМЕНЕ ЕЛЕКТРОЛИТИЧКЕ ОКСИДАЦИЈЕ

СТЕВАН СТОЈАДИНОВИЋ и РАСТКО ВАСИЛИЋ

Универзитет у Београду, Физички факултет, Студентски трг 12–16, 11000 Београд

У овом раду је испитивана плазмена електролитичка оксидација (ПЕО) Al–Zn–Si легуре (55 % Al, 43,5 % Zn, 1,5 % Si) у воденом раствору који садржи 4 g L^{-1} натријум-метасиликата, при константној густини струје од 400 mA cm^{-2}. Неутрални и јонизовани атоми који учествују у ПЕО микро-пражњењима су идентификовани техником оптичке емисионе спектроскопије. Испитивани ПЕО емисиони спектар се састоји од атомских и јонских линија које потичу од елемената присутних у подлози (Al, Zn) и електролиту (Na, O, H). Поред атомских и јонских линија, детектована је и AlO трака са максимумом на 484,2 nm. Густина електрона у плазми током микро-пражњења је процењена из анализе профила водоничне H_β линије. Електронска температура пражњења од 4000±400 K је процењена мерењем релативних интензитета атомских линија цинка на 481,05 и 636,23 nm. Поред тога, морфологија површине, хемијски и фазни састав оксидних слојева испитивани су помоћу SEM-EDS и XRD техника. Морфологија оксидних слојева зависи од времена ПЕО процеса, док Al, Zn, O и Si представљају главне хемијске елементе од којих су изграђени добијени оксидни слојеви. Оксидни слојеви су делимично кристализовани и углавном се састоје од гама фазе Al_2O_3.

(Примљено 18. априла, прихваћено 9. маја 2019)

REFERENCES

1. S. Stojadinović, R. Vasilić, I. Belča, M. Petković, B. Kasalica, Z. Nedić, Lj. Zeković, *Corros. Sci.* **52** (2010) 3258 (http://dx.doi.org/doi:10.1016/j.corsci.2010.05.042)
2. S. Stojadinović, R. Vasilić, J. Radić-Perić, M. Perić, *Surf. Coat. Technol.* **273** (2015) 1 (https://doi.org/10.1016/j.surfcoat.2015.03.032)
3. S. Stojadinović, R. Vasilić, M. Petković, B. Kasalica, I. Belča, A. Žekić, Lj. Zeković, *Appl. Surf. Sci.* **265** (2013) 226 (https://doi.org/10.1016/j.apsusc.2012.10.183)
4. M. Petković, S. Stojadinović, R. Vasilić, Lj. Zeković, *Appl. Surf. Sci.* **257** (2011) 10590 https://doi.org/10.1016/j.apsusc.2011.07.055
5. S. Stojadinović, R. Vasilić, *J. Alloys Compd.* **685** (2016) 881 (https://doi.org/10.1016/j.apsusc.2011.07.055)
6. S. Stojadinović, N. Tadić, R. Vasilić, *Int. J. Refract. Met. Hard Mater.* **69** (2017) 153 (http://dx.doi.org/10.1016/j.ijrmhm.2017.08.011)
7. S. Stojadinović, N. Tadić, R. Vasilić, *Surf. Coat. Technol.* **307** (2016) 650 (https://doi.org/10.1016/j.surfcoat.2016.09.080)
8. T. W. Clyne, S. C. Troughton, *Int. Mater. Rev.* **64** (2019) 127 (https://doi.org/10.1080/09506608.2018.1466492)
9. B. Kasalica, M. Petković, I. Belča, S. Stojadinović, Lj. Zeković, *Surf. Coat. Technol.* **203** (2009) 3000 (https://doi.org/10.1016/j.surfcoat.2009.03.038)
10. S. Stojadinović, J. Jovović, M. Petković, R. Vasilić, N. Konjević, *Surf. Coat. Technol.* **205** (2011) 5406 (https://doi.org/10.1016/j.surfcoat.2011.06.013)
11. J. Jovović, S. Stojadinović, N.M. Šišović, N. Konjević, *Surf. Coat. Technol*. **206** (2011) 24 (https://doi.org/10.1016/j.surfcoat.2011.06.031)

12. S. Stojadinović, R. Vasilić, M. Petković, Lj. Zeković, *Surf. Coat. Technol.* **206** (2011) 575 (https://doi.org/10.1016/j.surfcoat.2011.07.090)
13. S. Stojadinović, M. Perić, M. Petković, R. Vasilić, B. Kasalica, I. Belča, J. Radić-Perić, *Electrochim. Acta* **56** (2011) 10122 (https://doi.org/10.1016/j.electacta.2011.08.110)
14. S. Stojadinović, M. Perić, J. Radić-Perić, R. Vasilić, M. Petković, Lj. Zeković, *Surf. Coat.Technol.* **206** (2012) 2905 (https://doi.org/10.1016/j.surfcoat.2011.12.020)
15. J. Jovović, S. Stojadinović, N. M. Šišović, N. Konjević, *J. Quant. Spectrosc. Radiat. Transfer* **113** (2012) 1928 (https://doi.org/10.1016/j.jqsrt.2012.06.008)
16. S. Stojadinović, R. Vasilić, M. Petković, I. Belča, B. Kasalica, M. Perić, Lj. Zeković, *Electrochim. Acta* **59** (2012) 354 (https://doi.org/10.1016/j.electacta.2011.10.084)
17. S. Stojadinović, R. Vasilić, M. Petković, I. Belča, B. Kasalica, M. Perić, Lj. Zeković, *Electrochim. Acta* **79** (2012) 133 (https://doi.org/10.1016/j.electacta.2012.06.097)
18. S. Stojadinović, R. Vasilić, M. Petković, I. Belča, B. Kasalica, Lj. Zeković, *Electrochem. Commun.* **35** (2013) 22 (https://doi.org/10.1016/j.elecom.2013.07.031)
19. S. Stojadinović, J. Radić-Perić, R. Vasilić, M. Perić, *Appl. Spectrosc.* **68** (2014) 101 (https://doi.org/10.1366/13-07198)
20. S. Stojadinović, R. Vasilić, M. Perić, *RSC Adv.* **4** (2014) 25759. (https://doi.org/10.1039/c4ra03873h)
21. M. Sarvan, J. Radić-Perić, B. Kasalica, I. Belča, S. Stojadinović, M. Perić, *Surf. Coat. Technol.* **254** (2014) 270 (https://doi.org/10.1016/j.surfcoat.2014.06.029)
22. F. Mécuson, T. Czerwiec, T. Belmonte, L. Dujardin, A. Viola, G. Henrion, *Surf. Coat. Technol.* **200** (2005) 804. (https://doi.org/10.1016/j.surfcoat.2005.01.076)
23. R. O. Hussein, X. Nie, D. O. Northwood, A. Yerokhin, A. Matthews, *J. Phys., D: Appl. Phys.* **43** (2010) 105203 (https://doi.org/10.1088/0022-3727/43/10/105203)
24. R. O. Hussein, X. Nie, D. O. Northwood, *Surf. Coat. Technol.* **205** (2010) 1659 (https://doi.org/10.1016/j.surfcoat.2010.08.059)
25. R. O. Hussein, D. O. Northwood, X. Nie, *J. Vac. Sci. Technol., A* **28** (2010) 766 (https://doi.org/10.1116/1.3429583)
26. E. Matykina, R. Arrabal, P. Skeldon, G. E. Thompson, P. Belenguer, *Surf. Coat. Technol.* **205** (2010) 1668 (https://doi.org/10.1016/j.surfcoat.2010.05.014)
27. C. S. Dunleavy, I.O. Golosnoy, J.A. Curran, T.W. Clyne, *Surf. Coat. Technol.* **203** (2009) 3410 (https://doi.org/10.1016/j.surfcoat.2009.05.004)
28. M. Klapkiv, H. Nykyforchyn, V. Posuvailo, *Mater. Sci.* **30** (1995) 333 (https://doi.org/10.1007/BF00569685)
29. R. Ranković, S. Stojadinović, M. Sarvan, B. Kasalica, M. Krmar, J. Radić-Perić, M. Perić, *J. Serb. Chem. Soc.* **77** (2012) 1483 (https://doi:10.2298/JSC120912105R)
30. Q. Luo, Q. Li, J.Y. Zhang, H. S. Lu, L. Li, K. C. Chou, *J. Alloys Compd.* **646** (2015) 843 (https://doi.org/10.1016/j.jallcom.2015.05.257)
31. S. Stojadinović, I. Belča, M. Tadić, B. Kasalica, Z. Nedić, Lj. Zeković, *J. Electroanal. Chem.* **619–620** (2008) 125 (https://doi.org/10.1016/j.jelechem.2008.03.022)
32. https://www.nist.gov/pml/atomic-spectra-database, visited on Feb. 26th, 2019
33. S. Stojadinović, N. Tadić, N. Radić, P. Stefanov, B. Grbić, R. Vasilić, *Appl. Surf. Sci.* **355** (2015) 912 (https://doi.org/10.1016/j.apsusc.2015.07.174).